Journal of Power Sources 216 (2012) 162–168

Contents lists available at SciVerse ScienceDirect

Journal of Power Sources

journal homepage: www.elsevier.com/locate/jpowsour

Carbon-coated nanoclustered $LiMn_{0.71}Fe_{0.29}PO_4$ cathode for lithium-ion batteries

Minki Jo, HoChun Yoo, Yoon Seok Jung*, Jaephil Cho*

Interdisciplinary School of Green Energy, Ulsan National Institute of Science and Technology (UNIST), Ulsan 689-798, Republic of Korea

HIGHLIGHTS

- Carbon-coated nanoclustered $LiMn_{0.71}Fe_{0.29}PO_4$ were prepared.
- The clustered morphology resulted in improved tap density and volumetric capacity.
- The carbon-coated $LiMn_{0.71}Fe_{0.29}PO_4$ exhibited much better performance than the carbon-coated $LiMnPO_4$.
- The *ex-situ* surface analyses were carried out using Raman spectroscopy, TOF-SIMS, and ICP-OES.

ARTICLE INFO

Article history:
Received 28 March 2012
Received in revised form
24 April 2012
Accepted 21 May 2012
Available online 28 May 2012

Keywords:
Lithium-ion battery
Cathode
Nanoparticle
Polyol method
Olivine
Carbon-coating

ABSTRACT

Carbon-coated clustered $LiMn_{0.71}Fe_{0.29}PO_4$ (*c*-LMFP) nanoparticles are prepared from ball-milling with a mixture of ~40 nm thick LMFP nanoplates obtained by polyol method and carbon black. The clustered nanocomposite structure of *c*-LMFP turns out to have advantages of improved volumetric energy density and electrochemical performance. The *c*-LMFP exhibits increased tap density of 0.9 g cm^{-3}, compared with the as-prepared LMFP nanoplates (0.6 g cm^{-3}), providing with high volumetric discharge capacity of 243 mA h cm^{-3} at 0.1C and 128 mA h cm^{-3} even at 7C at 21 °C. At elevated temperature (60 °C), the capacity retention of *c*-LMFP remains excellent (100% of its initial capacity (165 mA h g^{-1}) at the same cycling condition as 21 °C). In sharp contrast, capacity of carbon-coated $LiMnPO_4$ (*c*-LMP) exhibits volumetric discharge capacity of 72 mA h cm^{-3} at 5C and decays rapidly at 60 °C after 40 cycles (capacity retention of 58%). The better cycling stability of *c*-LMFP than that of *c*-LMP is believed to be associated with mitigated Mn^{2+} dissolution by Fe^{2+} substitution.

1. Introduction

Lithium transition metal oxides represented by layered $LiMO_2$ (M = Co, Ni, Mn) and spinel $LiMn_2O_4$ have been adopted as main cathode materials for the commercial lithium-ion batteries (LIBs) [1–3]. Since a pioneering work by Padhi et al. in 1997 [4], olivine $LiMPO_4$ (M = Fe, Mn, Co, etc) has been emerging as alternatives for the conventional oxide cathode materials [5,6]. Among them, much research efforts have focused on $LiFePO_4$ (LFP) because of its low cost, environmental benignity, and thermal stability originated from strong P–O bonds [4–6]. An intrinsic problem of low conductivity of LFP was successfully solved by synthesizing nano-sized particles and by surface-coating with carbon [5–11]. Although low operating potential of LFP (3.4 V *vs.* Li/Li^+) is sometimes regarded as benefit in terms of negligible side reaction associated with oxidative electrolyte decomposition, it clearly indicates low energy density which limits application for electric vehicles such as hybrid electric vehicles (HEVs) and plug-in HEVs (PHEVs). Accordingly, $LiMnPO_4$ (LMP) which has high operating potential of 4.1 V *vs.* Li/Li^+ has attracted much attention [4,12–19]. However, LMP suffers from five orders of magnitude lower electronic conductivity than LFP [20]. Compared with LFP, high operating potential of LMP would pose another possible concern on side reaction at high potential which will get severer at elevated temperature. However, much study on the issue of the side reaction has not been carried out extensively yet.

Recently, Martha et al. have demonstrated improved capacity and rate capability by partial substitution of Mn^{2+} in LMP by Fe^{2+} [21]. Since then, numerous synthetic methods to obtain nanostructures of LMFP have been tried [22–25]. The synthetic strategies to achieve favorable nanostructures of LFP and or LMP with carbon coating can be categorized by solid state synthesis, precipitation methods followed by heat treatment, hydro/solvothermal synthesis, low temperature precipitation methods, polyol synthesis, ionothermal synthesis, template methods, microwave-

* Corresponding authors. Tel.: +82 52 217 2910; fax: +82 52 217 2909.
E-mail addresses: ysjung@unist.ac.kr, yoonseok.jung@gmail.com (Y.S. Jung), jpcho@unist.ac.kr (J. Cho).

0378-7753/$ – see front matter © 2012 Elsevier B.V. All rights reserved.
doi:10.1016/j.jpowsour.2012.05.059

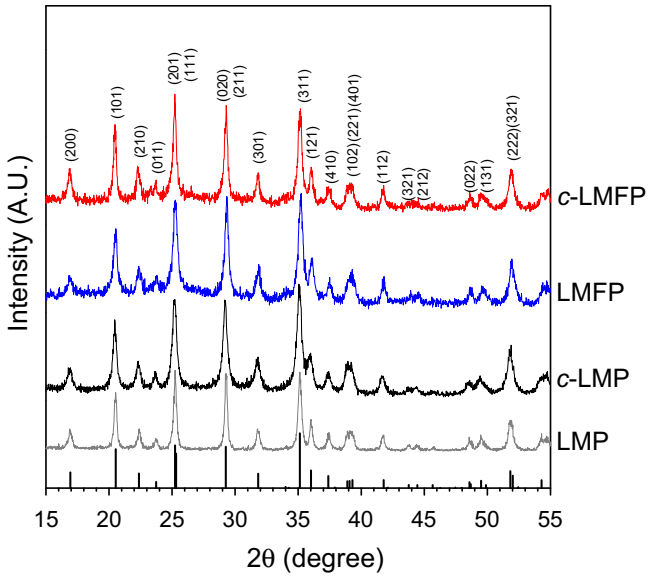

Fig. 1. XRD patterns of pristine and carbon-coated $LiMnPO_4$ and $LiMn_{0.71}Fe_{0.29}PO_4$. Reference peak (JCPDS no. 83–2092) is given in the bottom.

assisted syntheses, and etc [6]. Among them, the polyol synthesis is attractive because it enables formation of nanoparticles with good crystallinity at very low temperature [17,26–28]. To our knowledge, the polyol method has been applied for carbon-coated pure LFP and LMP so far [6,17,29–31], and the importance of volumetric capacity cannot be ignored due to the limited volume of LIBs.

Table 1
Lattice parameters of pristine and carbon-coated LMP and LMFP powders.

Sample name	*a* (Å)	*b* (Å)	*c* (Å)
Pristine LMP	10.4418	6.0936	4.7438
Carbon-coated LMP	10.4408	6.0870	4.7425
Pristine LMFP	10.4210	6.0806	4.7381
Carbon-coated LMFP	10.4211	6.0799	4.7331

Here, we report on carbon-coated clustered $LiMn_{0.71}Fe_{0.29}PO_4$ nanoparticles (cluster size of <40 μm) prepared by polyol method followed by carbon coating via ball-milling, showing high volumetric capacity of 128 mA h cm^{-3} even at 7C rate. In addition, after 40 cycles at 0.1C at elevated temperature (60 °C), the clustered *c*-LMFP exhibits excellent performance with the capacity retention of 100%. The electrochemical performances at different temperatures (21 °C and 60 °C) are also presented compared with counter reference, carbon-coated $LiMnPO_4$.

2. Experimental

2.1. Preparation of LMP and LMFP powders

The LMP and LMFP nanoplates were prepared by polyol method. For LMP, 30 mL aqueous solution of 60 mM manganese(II) acetate tetrahydrate ($Mn(CH_3COO)_2{\cdot}4H_2O$, 99%, Aldrich) was mixed with 200 mL of tetra(ethylene glycol) (TTEG). For LMFP, 30 mL aqueous solution of 42 mM manganese(II) acetate tetrahydrate and 18 mM iron(II) acetylacetonate ($[CH_3COCH{=}C(O)CH_3]_2Fe$, 99%, Aldrich) was mixed with 200 mL TTEG. After each mixed solution was

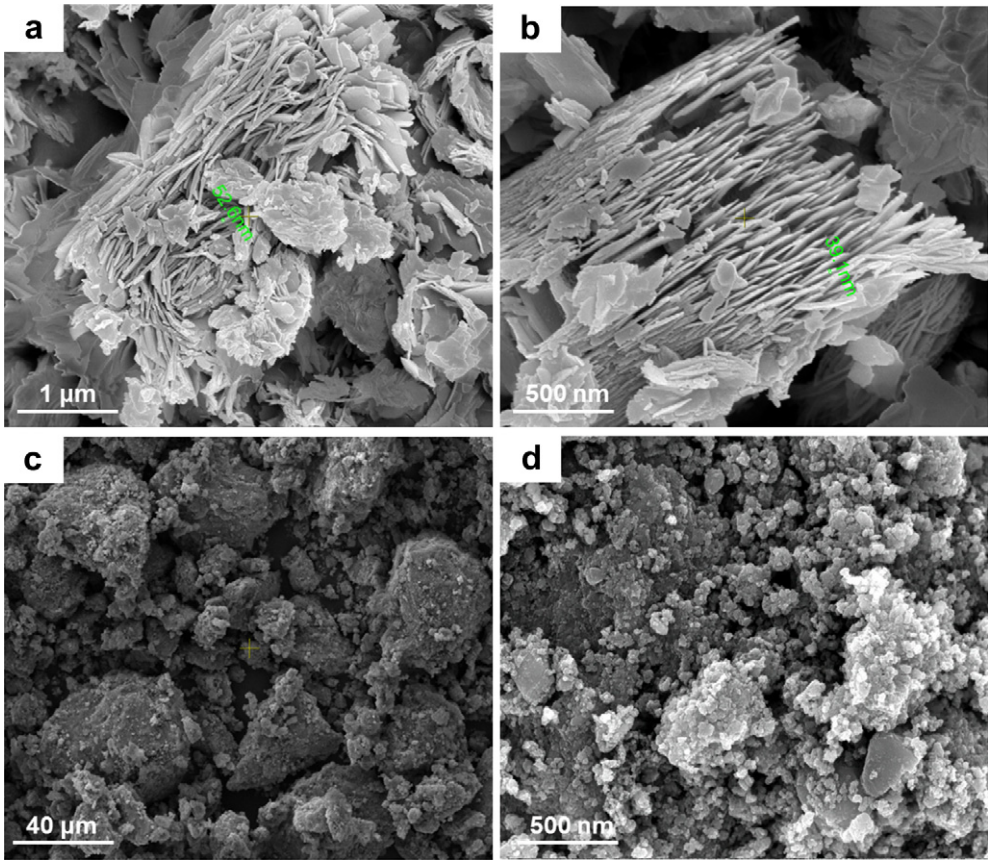

Fig. 2. SEM images of (a) pristine (before ball-milling) LMFP particles, (b) magnified image of (a), (c) carbon-coated (after ball-milling) LMFP particles, (d) magnified image of (c).

vigorously stirred in three-neck round flask and heated at 100 °C (solution temperature) for 1 h, 30 mL of 2 M lithium dihydrogenphosphate (LiH_2PO_4, 99%, Aldrich) aqueous solution was added dropwise into the mixed solution. The solution was kept at 100 °C for 4 h and cooled to room temperature. The resulting LMP and LMFP particles were filtered and washed four times with ethanol and dried under vacuum at 120 °C overnight. Carbon-coating was carried out by ball-milling of 80 wt% of LMP or LMFP powders with 20 wt% of carbon (Ketjen black) with 300 rpm for 4 h using planetary mono mill, Pulverisette 6 (Fritsch CmbH). A stainless steel container (200 mL) and balls were used with a weight ratio of 1:30 (mixed powder:balls). The container was assembled in a glove box filled with pure Ar.

2.2. Materials characterization

Powder X-ray diffraction (XRD) measurement using Cu K_α radiation was carried out using D/Max2000 (Rigaku). Morphology was examined by using scanning electron microscopy (SEM) (JSM 6400, JEOL) and transmission electron microscopy (TEM) (JEOL 2010F). Raman spectroscopy measurements were performed using an Alpha300R (WITec, USA). A He–Ne laser operating at $\lambda = 532$ nm was used as the excitation source. The composition of LMFP was determined by inductively coupled plasma optical emission spectroscopy (ICP-OES) (720-ES, Varian, USA). The amount of dissolved Mn in the electrolyte was also measured by ICP-OES.

Time-of-flight secondary ion mass spectrometry (TOF-SIMS) measurements were performed with TOF-SIMS V(ION TOF, Germany) which used a 25 keV Bi^{3+} primary ion-gun. The primary ion beam was rastered on 20×20 μm^2 areas with a current of 0.1 pA.

2.3. Electrochemical characterization

Electrodes comprised of active materials (*c*-LMP or *c*-LMFP), Super P as a conductive additive, and poly(vinylidene fluoride) (PVdF) as a binder (85:5:10 weight ratio) were fabricated. Thickness of the electrodes was ca. 40 μm and loading amount of active materials was 6–7 mg cm^{-2}. Charge-discharge cycling tests were performed between 4.6 and 2.0 V (*vs.* Li/Li^+) with constant current-constant voltage (cccv) mode (constant voltage for 2.5 h) for charge and with constant current for discharge at two different temperatures (21 °C and 60 °C) using coin-type half cells. Li metal was used as a counter and reference electrode. 1.1 M $LiPF_6$ dissolved in a mixed solvent of ethylene carbonate (EC) and diethyl carbonate (DEC) (1:1 vol. ratio) was used as an electrolyte.

3. Results and discussion

The ball-milling with carbon is one of the most cost-effective and efficient methods to achieve good carbon-coatings as seen in many previous works regarding the olivine cathodes [13,15,16,20,23,27]. Fig. 1 shows the powder XRD patterns of

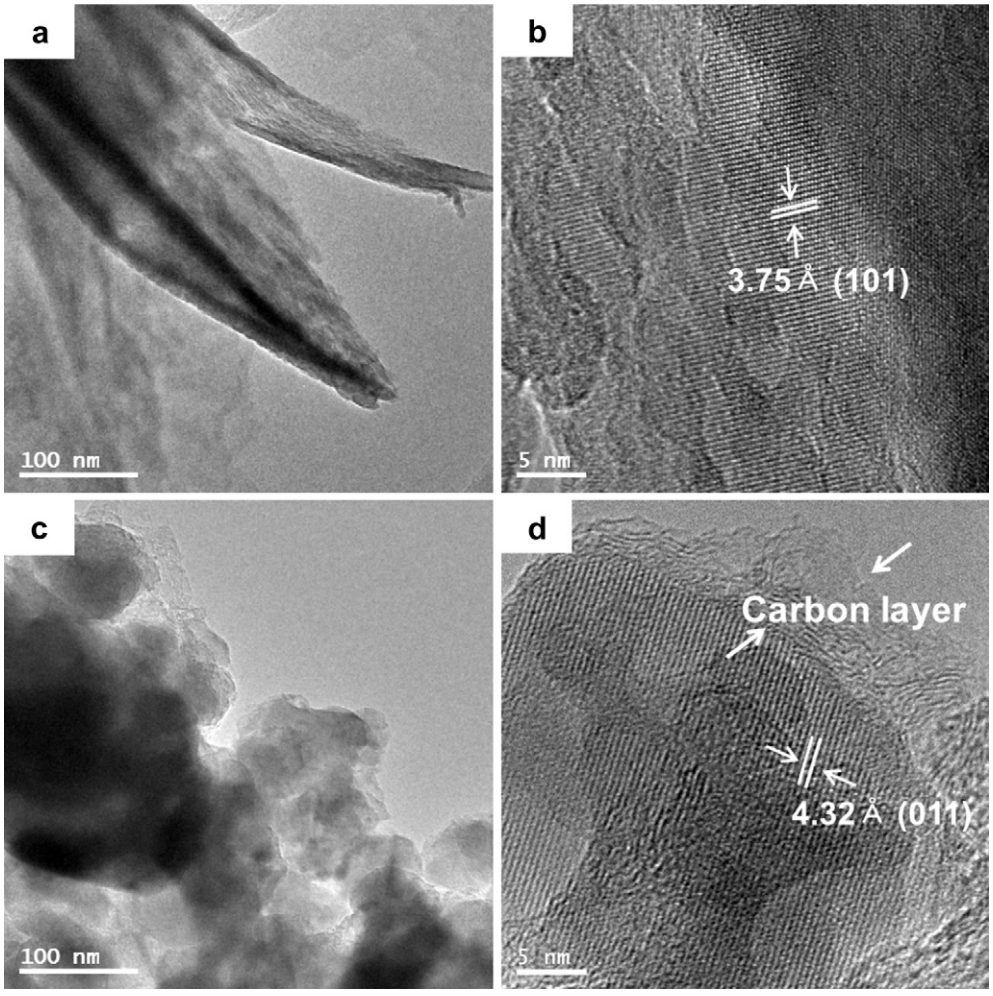

Fig. 3. TEM images of (a) pristine and (c) carbon-coated LMFP particles and HRTEM images of (b) pristine and (d) carbon-coated LMFP particles.

pristine and carbon-coated LMP and LMFP powders. The peaks of the pristine sample correspond well with olivine structure of P*nma* orthorhombic system [32]. After the carbon-coating via ball-milling, the peak position and shape does not change significantly, indicating that the ball-milling does not destroy the original crystalline structure. The lattice parameters of the pristine and carbon-coated LMP and LMFP compared in Table 1 also shows very slight change after the carbon-coating, which again satisfies only marginal effects of the ball-milling on the crystal structure. The calculated lattice parameters of carbon-coated LMFP (*c*-LMFP) is $a = 10.4211$Å, $b = 6.0799$ Å, and $c = 4.7331$ Å, which reflects a compressed unit cell compared with those of carbon-coated $LiMnPO_4$ (*c*-LMP), $a = 10.4408$ Å, $b = 6.0870$ Å, and $c = 4.7425$ Å. This observation is associated with smaller ionic radii of Fe^{2+} (0.92 Å) than that of Mn^{2+} (0.97 Å) [33]. It is also noticeable that the peak ratios of the synthesized LMFP powders are different from those of the standard one. The fact that the peak ratio of (020)/(311) for the standard file is 0.78 [17], while the ones for the synthesized LMFP is higher (0.9 and 1.0 for pristine and carbon-coated LMFP, respectively) implies that the nanoplates are oriented in the *a*-*c* plane. This should be favorable for the Li^+-ion diffusion because the diffusion occurs only in the shortest *b* direction.

The morphologies of pristine and carbon-coated LMFP by SEM are displayed in Fig. 2. The pristine LMFP exhibits nanoplate shapes with thickness of ca. 40 nm, which is consistent with those of pure LFP or LMP obtained by polyol method in the previous reports [17,27,31]. This resulting morphology can allow fast Li^+-ion diffusion, thereby mitigating the extremely slow kinetics of LMFP. However, there still exist two problems that should be further overcome. First, an electronically conductive surface coating or wiring is needed due to still extremely low electronic conductivity of LMFP. Second, the nanoplates morphology gives very porous structure, resulting in very low tap density (0.6 g cm^{-3}). This feature significantly lowers volumetric capacity or energy density. In a sharp contrast, after the carbon coating via ball-milling, the resulting materials display relatively dense structure where primary nanoparticles are clustered, forming secondary particles with a size of <40 μm. Even though the *c*-LMFP contains 20 wt.% of carbon, tap density is significantly increased (0.9 g cm^{-3}). Accordingly, an electrode density of *c*-LMFP is higher (1.5 g cm^{-3}) than that of the pristine LMFP (1.3 g cm^{-3}). Additionally, it is expected that the added carbon can mitigate the poor electronic conductivity problem of LMFP domain. As evidenced by TEM and HRTEM images of pristine LMFP and *c*-LMFP (Fig. 3), amorphous carbon layers well coat the surface of LMFP nanocrystals with thicknesses of a few to tens of nm. Also the lattice fringes of LMFP well supports that the ball-milling does not destroy the crystal structure of LMFP.

Fig. 4a and b presents the first charge-discharge voltage curves of *c*-LMP and *c*-LMFP at 0.1C at 21 °C. The cells were charged to 4.6 V in a cccv mode (held at 4.6 V for 2.5 h) and discharged to 2.0 V. The *c*-LMP exhibits a single plateau centered at ~4.1 V during charge and discharge, which is related to the Mn^{2+}/Mn^{3+} redox couples. In contrast, *c*-LMFP shows an additional small plateau at ~3.5 V associated with the Fe^{2+}/Fe^{3+} redox couples [4]. First differential charge-discharge voltage profiles derived from the first charge-discharge voltage profiles are displayed in Fig. 4c. Consistent with Fig. 4a and b, the Mn^{2+}/Mn^{3+} redox peaks are seen at ~4.1 V. Importantly, compared with *c*-LMP, *c*-LMFP exhibits smaller difference in the charge and discharge peaks of Mn^{2+}/Mn^{3+}, implying lowered polarization. Also the reversible capacities of *c*-LMFP are much higher than those of *c*-LMP as seen in Fig. 4a and b. For example, the first discharge capacity of *c*-LMFP at 0.1C (Fig. 4b) is 162 mA h g^{-1} while that of *c*-LMP is 114 mA h g^{-1} (Fig. 4a). These observations of smaller polarization and higher capacities of *c*-LMFP than those of *c*-LMP reflects positive effect of Fe^{2+} substitution, which may be originated from increased electronic conductivity [27] and or improved Li^+-ion diffusion.

As seen in Fig. 5a, the rate performance of *c*-LMFP was measured by charging the *c*-LMFP/Li half cell to 4.6 V in cccv mode at 0.1C and discharging with varied C-rates at 21 °C. The *c*-LMFP delivers a discharge capacity of 111 mA h g^{-1} at 5C, showing the capacity retention of 71% compared with that of 0.1C. On the other hand, the *c*-LMP delivers a discharge capacity of 72 mA h g^{-1} at 5C with the capacity retention of 60% (Fig. 5b). In addition, the discharge capacity of *c*-LMFP shows 128 mA h g^{-1} at 3C, which is higher than that obtained from the micro-sized $LiMn_{0.85}Fe_{0.15}PO_4$ via co-precipitation method (~100 mA h g^{-1}) [34]. Fig. 5c shows the volumetric capacities based on the electrode densities of *c*-LMP and *c*-LMFP (1.3 g cm^{-3} and 1.5 g cm^{-3}, respectively). The *c*-LMFP delivers much higher volumetric capacity of 243 mA h cm^{-3} at 0.1C than that of the *c*-LMP (162 mA h cm^{-3}). Moreover, 54% of the capacity (128 mA h cm^{-3}) is retained even at 7C. Volumetric capacity is one of the most important factors for the practical Li-ion cells because it determines the amount of the loaded active material. In this regard, the high volumetric capacity with high rate capability obtained in this work is promising.

Cycling performances of *c*-LMFP and *c*-LMP were measured at two different C-rates (0.1C and 1C) at two different temperatures (21 °C and 60 °C) as displayed in Fig. 6. At 21 °C (Fig. 6a), although *c*-LMP shows lower capacities than those of *c*-LMFP, both exhibits

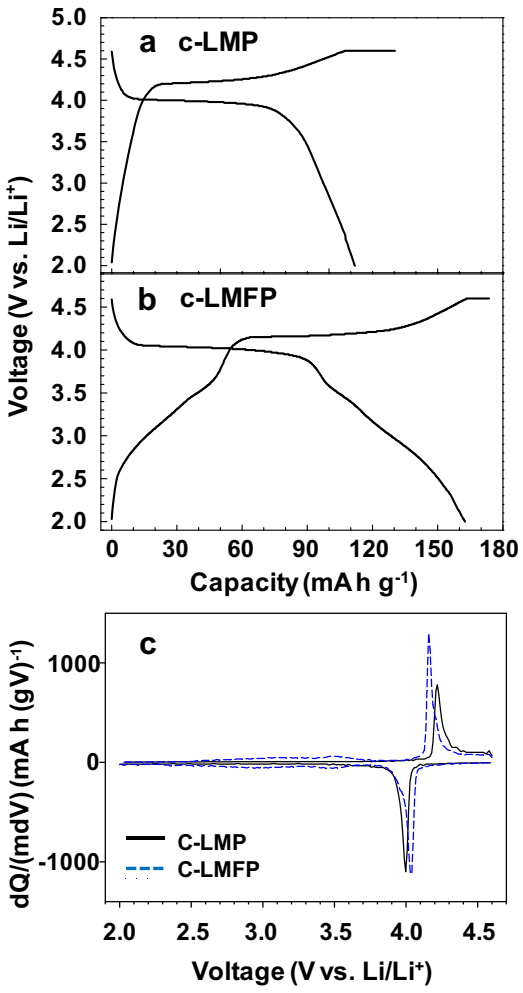

Fig. 4. First charge-discharge voltage profiles of (a) *c*-LMP and (b) *c*-LMFP at 0.1C at 21 °C and (c) corresponding d*Q*/d*V* curves.

stable cycling performances, implying reversible redox reactions. It is noted that even though *c*-LMP suffers from low capacity, it shows stable cycling performance, which may support that Jahn-Teller distortion may not be responsible for the performance of LMP in contrary to the spinel $LiMn_2O_4$ [17]. At elevated temperature (60 °C), however, the *c*-LMFP retains 100% and 89% of its initial capacities after 40 cycles at 0.1C and 1C, respectively, while the *c*-LMP retains only 58% and 29% of its initial capacities. The dramatically improved cycling stability at high temperature observed in LMFP compared with LMP should be another important benefit by Fe^{2+} substitution.

Due to the higher operating potential of LMFP (~4.1 V) than that of LFP (~3.5 V), the electrode–electrolyte interface stability may be more critical for LMFP than LFP. This situation becomes even more critical at high temperature where not only the main redox reaction but also undesirable side reactions are accelerated. In an attempt to estimate the side reaction as a function of voltage, *ex situ* Raman spectroscopy after charging *c*-LMFP at 3.4 V and 4.4 V at 60 °C were obtained (Fig. 7). A strong peak at ~950 cm^{-1} and another peak at ~1000 cm^{-1} are associated with the vibrations of the phosphate anions in the olivine structure [35]. It is also clearly seen that the signatures of Li_2CO_3 (~710 cm^{-1} and 1095 cm^{-1}) [36] which is one of the most common components of the solid electrolyte interphase (SEI) are not shown at lower potential (3.4 V), but appears at higher potential (4.4 V). An unknown peak ('?') at ~1035 cm^{-1}may come from one of the SEI components in that it appears only at high potential, 4.4 V. These observations strongly

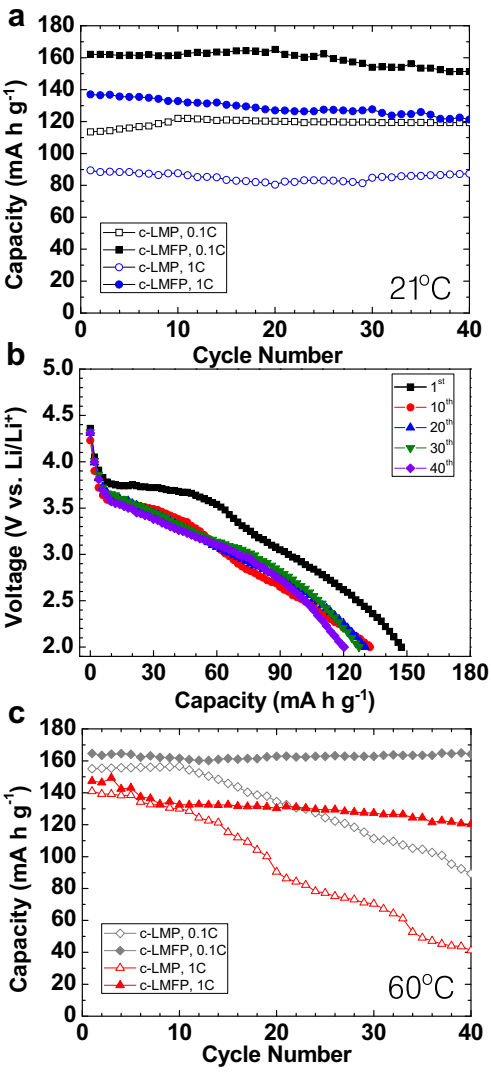

Fig. 6. (a) Cycling performance of *c*-LMP and *c*-LMFP at 0.1C and 1C at 21 °C. (b) Discharge voltage profiles of *c*-LMFP at 1C at 60 °C. (c) Cycling performance of *c*-LMP and *c*-LMFP at 0.1C and 1C at 60 °C.

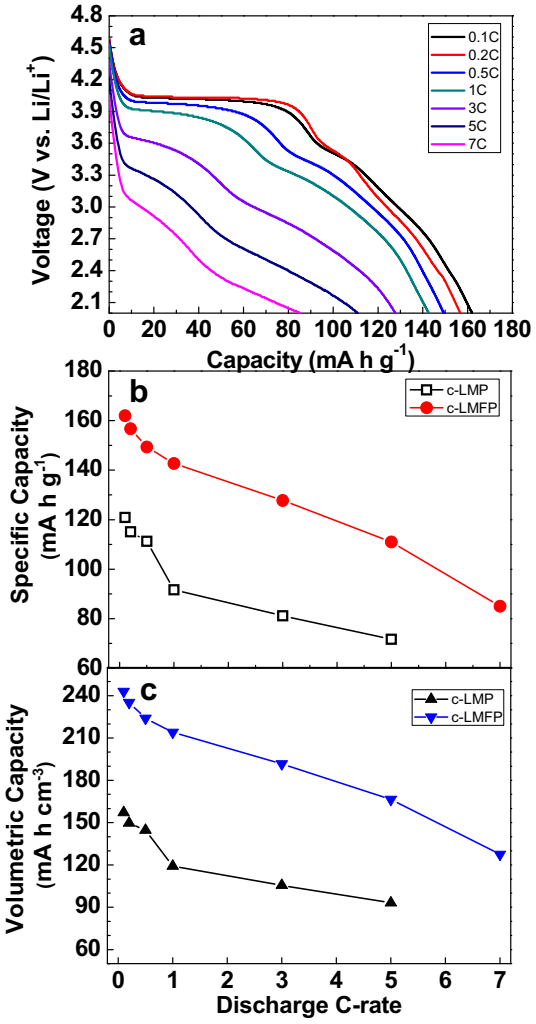

Fig. 5. (a) Discharge voltage profiles of *c*-LMFP at different C-rates at21 °C. (b) Specific and (c) volumetric capacity of *c*-LMP and *c*-LMFP as a function of discharge C-rate. The cells were charged up to 4.6 V in cccv mode at 0.1C.

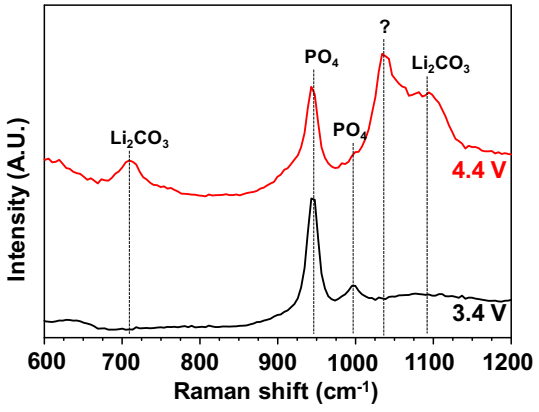

Fig. 7. *Ex-situ* Raman spectra of *c*-LMFP electrodes after delithiation (charge) up to given potential (inset) at 60 °C.

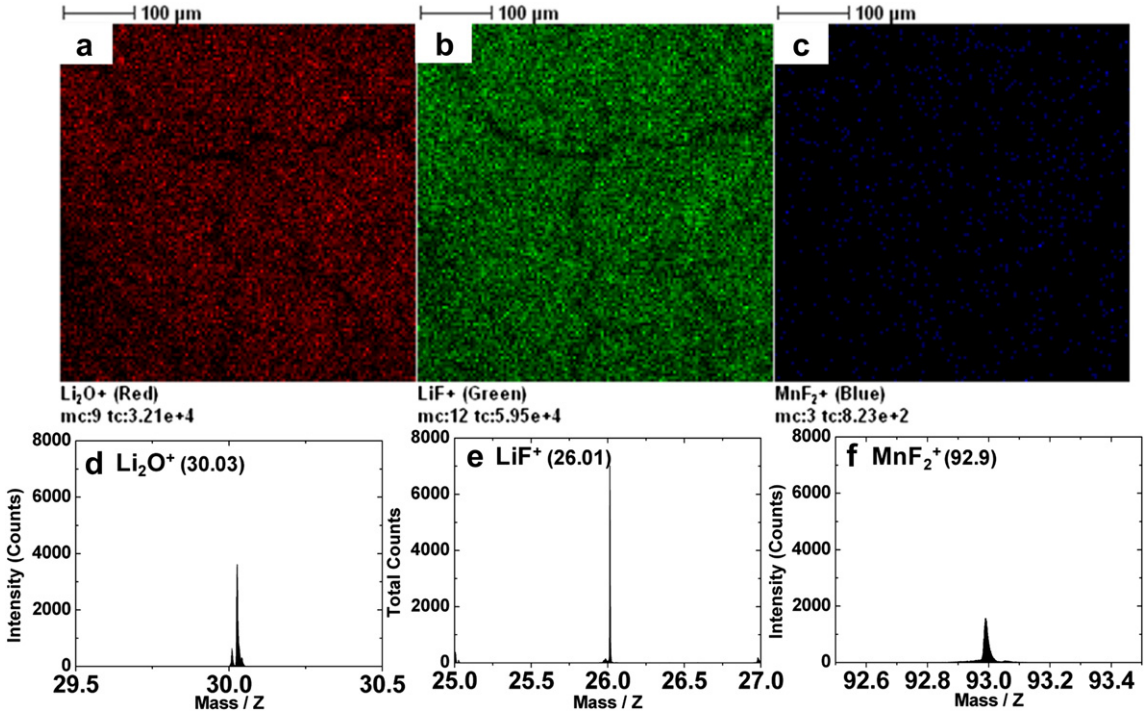

Fig. 8. TOF-SIMS images (a–c) and spectra (d–f) of the c-LMFP electrode after 40 cycles at 0.1C at 60 °C; (a, d) Li_2O^+, (b, e) LiF^+, and (c, f) MnF_2^+.

support that LMFP may suffer from undesirable surface reaction at high potential and at elevated temperature. The TOF-SIMS results in Fig. 8 also confirm the existence of byproducts on the surface of the*c*-LMFP electrode after 40 cycles at 0.1C at elevated temperature (60 °C). Li_2O (Fig. 8a and d) and LiF (Fig. 8b and e) are typical components of the SEI on electrodes[37]. The existence of MnF_2(Fig. 8c and f) may reflect redeposition of the dissolved Mn ions [38,39], which supports the speculation that the surface reaction of LMP or LMFP may be closely related to the Mn^{2+}dissolution like the case of spinel $LiMn_2O_4$ [23,40].

Thus, the rapid capacity decay of *c*-LMP at elevated temperature in Fig. 7b should be associated with the undesirable surface reactions in that the operating potential of LMP is same as that of LMFP. The significantly improved performance of *c*-LMFP compared with that of *c*-LMP in Fig. 6 implies that the substituted Fe^{2+} may affect the surface side reaction. The dissolved amount of Mn ions of *c*-LMP and *c*-LMFP were obtained after storing the charged electrode (4.6 V) in the electrolyte at 60 °C for 21 days. The amount of dissolved Mn ions in *c*-LMFP (3.58 ppm) is much lower than that in *c*-LMP (18.6 ppm), indicating Fe^{2+} substitution suppresses the Mn^{2+}-ion dissolution. This observation suggests that the improved performance of *c*-LMFP than *c*-LMP may be closely related to the surface side reactions rather than the structural effect of the bulk.

4. Conclusions

Carbon-coated clustered $LiMn_{0.71}Fe_{0.29}PO_4$ nanoparticles with a size of<40 μm were prepared as cathode materials by polyol method followed by ball-milling. The resulting nanostructures provided with better electronic conductivity and higher tap density (0.9 g cm^{-3}) with maintaining the original crystallinity. The *c*-LMFP showed high volumetric capacity of 243 mA h cm^{-3} at 0.1C at 21 °C, high rate capability of 128 mA h cm^{-3} even at 7C, and excellent cycling performance with the capacity retention of 100% especially at high temperature (after 40 cycles at 0.1C at 60 °C). The much better cycling stability of *c*-LMFP than that of *c*-LMP at elevated temperature was suggested to be related to the mitigated Mn^{2+}-ion dissolution.

Acknowledgments

This research was supported by the MKE (The Ministry of Knowledge Economy), Korea, under the ITRC (Information Technology Research Center) support program supervised by the NIPA(National IT Industry Promotion Agency)" (NIPA-2012-C1090-1200-0002).

References

[1] M.S. Whittingham, Chem. Rev. 104 (2004) 4271–4301.
[2] J.B. Goodenough, Y. Kim, Chem. Mater. 22 (2009) 587–603.
[3] B.L. Ellis, K.T. Lee, L.F. Nazar, Chem. Mater. 22 (2010) 691–714.
[4] A.K. Padhi, K.S. Nanjundaswamy, J.B. Goodenough, J. Electrochem. Soc. 144 (1997) 1188–1194.
[5] L.-X. Yuan, Z.-H. Wang, W.-X. Zhang, X.-L. Hu, J.-T. Chen, Y.-H. Huang, J.B. Goodenough, Energy Environ. Sci. 4 (2011) 269–284.
[6] H.K. Song, K.T. Lee, M.G. Kim, L.F. Nazar, J. Cho, Adv. Funct. Mater. 20 (2010) 3818–3834.
[7] N. Ravet, Y. Chouinard, J.F. Magnan, S. Besner, M. Gauthier, M. Armand, J. Power Sources 97-8 (2001) 503–507.
[8] P.P. Prosini, M. Carewska, S. Scaccia, P. Wisniewski, M. Pasquali, Electrochim. Acta 48 (2003) 4205–4211.
[9] P.S. Herle, B. Ellis, N. Coombs, L.F. Nazar, Nat. Mater. 3 (2004) 147–152.
[10] A. Singhal, G. Skandan, G. Amatucci, F. Badway, N. Ye, A. Manthiram, H. Ye, J.J. Xu, J. Power Sources 129 (2004) 38–44.
[11] M. Gaberscek, R. Dominko, J. Jamnik, Electrochem. Commun. 9 (2007) 2778–2783.
[12] G.H. Li, H. Azuma, M. Tohda, Electrochem. Solid-State Lett. 5 (2002) A135–A137.
[13] C. Delacourt, P. Poizot, M. Morcrette, J.M. Tarascon, C. Masquelier, Chem. Mater. 16 (2004) 93–99.
[14] R. Dominko, M. Bele, M. Gaberscek, M. Remskar, D. Hanzel, J.M. Goupil, S. Pejovnik, J. Jamnik, J. Power Sources 153 (2006) 274–280.
[15] N.H. Kwon, T. Drezen, I. Exnar, I. Teerlinck, M. Isono, M. Graetzel, Electrochem. Solid-State Lett. 9 (2006) A277–A280.
[16] T. Drezen, N.H. Kwon, P. Bowen, I. Teerlinck, M. Isono, I. Exnar, J. Power Sources 174 (2007) 949–953.
[17] D.Y. Wang, H. Buqa, M. Crouzet, G. Deghenghi, T. Drezen, I. Exnar, N.H. Kwon, J.H. Miners, L. Poletto, M. Graetzel, J. Power Sources 189 (2009) 624–628.

[18] D. Choi, D. Wang, I.-T. Bae, J. Xiao, Z. Nie, W. Wang, V.V. Viswanathan, Y.J. Lee, J.-G. Zhang, G.L. Graff, Z. Yang, J. Liu, Nano Lett. 10 (2010) 2799–2805.
[19] H. Yoo, M. Jo, B.S. Jin, H.S. Kim, J. Cho, Adv. Energy Mater. 1 (2011) 347–351.
[20] C. Delacourt, C. Wurm, L. Laffont, J.B. Leriche, C. Masquelier, Solid State Ionics 177 (2006) 333–341.
[21] S.K. Martha, J. Grinblat, O. Haik, E. Zinigrad, T. Drezen, J.H. Miners, I. Exnar, A. Kay, B. Markovsky, D. Aurbach, Angew. Chem. Int. Ed. 48 (2009) 8559–8563.
[22] B. Zhang, X.J. Wang, Z.J. Liu, H. Li, X.J. Huang, J. Electrochem. Soc. 157 (2010) A285–A288.
[23] S.M. Oh, H.G. Jung, C.S. Yoon, S.T. Myung, Z.H. Chen, K. Amine, Y.K. Sun, J. Power Sources 196 (2011) 6924–6928.
[24] J.A. Hong, F. Wang, X.L. Wang, J. Graetz, J. Power Sources 196 (2011) 3659–3663.
[25] H. Wang, Y. Yang, Y. Liang, L.-F. Cui, H. Sanchez Casalongue, Y. Li, G. Hong, Y. Cui, H. Dai, Angew. Chem. Int. Ed. 50 (2011) 7364–7368.
[26] T.R. Kim, D.H. Kim, H.W. Ryu, J.H. Moon, J.H. Lee, S. Boo, J. Kim, J. Phys. Chem. Solids 68 (2007) 1203–1206.
[27] S.K. Martha, B. Markovsky, J. Grinblat, Y. Gofer, O. Haik, E. Zinigrad, D. Aurbach, T. Drezen, D. Wang, G. Deghenghi, I. Exnar, J. Electrochem. Soc. 156 (2009) A541–A552.
[28] D. Kim, J. Lim, E. Choi, J. Gim, V. Mathew, Y. Paik, H. Jung, W. Lee, D. Ahn, S. Paek, J. Kim, Surf. Rev. Lett. 17 (2010) 111–119.
[29] P.R. Kumar, M. Venkateswarlu, M. Misra, A.K. Mohanty, N. Satyanarayana, J. Electrochem. Soc. 158 (2011) A227–A230.
[30] E.S. Choi, D.H. Kim, C.H. Woo, C.H. Choi, J. Kim, J. Nanosci. Nanotechnol. 10 (2010) 3416–3419.
[31] J.S. Lim, D.H. Kim, I.O. Jung, C.H. Woo, E.S. Choi, J.H. Gim, J. Kim, J. Nanosci. Nanotechnol. 10 (2010) 3357–3361.
[32] A. Yamada, S.-C. Chung, J. Electrochem. Soc. 148 (2001) A960–A967.
[33] R.D. Shannon, Acta Crystallogr. Sect. A 32 (1976) 751–767.
[34] Y.K. Sun, S.M. Oh, H.K. Park, B. Scrosati, Adv. Mater. 23 (2011) 5050–5054.
[35] E. Markevich, R. Sharabi, O. Haik, V. Borgel, G. Salitra, D. Aurbach, G. Semrau, M.A. Schmidt, N. Schall, C. Stinner, J. Power Sources 196 (2011) 6433–6439.
[36] N. Koura, S. Kohara, K. Takeuchi, S. Takahashi, L.A. Curtiss, M. Grimsditch, M.L. Saboungi, J. Mol. Struct. 382 (1996) 163–169.
[37] T.T. Fister, M. Schmidt, P. Fenter, C.S. Johnson, M.D. Slater, J. Chem. Phys. 135 (2011) 224513/1–224513/5.
[38] Y.K. Sun, S.T. Myung, B.C. Park, H. Yashiro, J. Electrochem. Soc. 155 (2008) A705–A710.
[39] D. Kim, S. Park, O.B. Chae, J.H. Ryu, Y.-U. Kim, R.-Z. Yin, S.M. Oh, J. Electrochem. Soc. 159 (2012) A193–A197.
[40] D.H. Jang, Y.J. Shin, S.M. Oh, J. Electrochem. Soc. 143 (1996) 2204–2211.